Modeling photon-induced reactions on $^{233–238}$U actinide targets

M. Sin,[1] R. Capote,[2,*] M. W. Herman,[3] A. Trkov,[2] and B. V. Carlson[4]
[1]*University of Bucharest, Faculty of Physics, Bucharest-Magurele, RO-077125, Romania*
[2]*NAPC–Nuclear Data Section, International Atomic Energy Agency, A-1400 Vienna, Austria*
[3]*Los Alamos National Laboratory, Los Alamos, New Mexico 87544, USA*
[4]*Instituto Tecnológico de Aeronáutica, Brazil*

(Received 25 September 2019; revised 3 January 2021; accepted 10 March 2021; published 10 May 2021)

Comprehensive calculations of photon-induced reactions on $^{233–238}$U targets for incident photon energies from 3 up to 30 MeV are undertaken with the statistical model code EMPIRE-3.2 Malta. Results are compared with the experimental data from EXFOR and with the current evaluations. The differences and the similarities between the models and parameters used in calculations of photon- and neutron-induced reactions on the same nuclei are discussed with focus on fission. The role of the extended optical model for fission that includes partial damping in the continuum in improving the description of the measured data is pointed out.

DOI: 10.1103/PhysRevC.103.054605

I. INTRODUCTION

The fission model and model parameters represent the largest source of uncertainty when performing model reaction calculations for actinide targets.

To address this issue, the International Agency for Atomic Energy is coordinating an ongoing research project to deliver comprehensive sets of fission parameters and corresponding well-documented models [1]. Newly proposed parametrized models are expected to enhance the use of modeling in evaluation practice and to meet target uncertainties for applications.

As pointed out in Ref. [2], "a consistent and reliable set of fission parameters as model independent as possible is the one which provides simultaneously a reasonable description of multiple fission chances induced by neutrons, photons, protons or direct transfer reactions leading to the same fissionable compound nucleus." Such consistent sets of fission parameters have been obtained for the uranium isotopic chain from the simultaneous description of the experimental neutron-induced reactions cross sections and Neutron Standard cross sections [3,4] by model calculations in Refs. [2,5–7]. The evaluations based on those calculations for ^{235}U and ^{238}U have been produced within the NEA CIELO project [8,9], and have been adopted by the ENDF/B-VIII.0 library [10]. Similar calculations of neutron-induced reactions on the whole Uranium isotopic chain have been performed by several groups along the years, and can be found in Refs. [11–16].

A new step in obtaining "consistent and reliable" sets of fission parameters for the Uranium isotopes is addressed in this work by testing the compatibility of the fission parameters deduced from the fit of the neutron induced fission cross sections in Ref. [2] with the input parameters specific to photon-induced reaction modeling. For this purpose, photon-induced reaction cross section calculations for $^{233–238}$U have been performed with the statistical model code EMPIRE-3.2 Malta [17,18] in the incident energy range 3–30 MeV.

Photon-induced reactions are important for a large range of applications from radiotherapy and astrophysics to transmutation of nuclear waste, forensics or shielding. They provide useful information for the data evaluation of reactions induced by other particles, the most known and important being the photon strength functions, involved in the calculation of capture cross section, isomeric state population, gamma spectra, and so on. As discussed in this paper, the photoreactions also allow us to explore the fission barriers at low energies. In the last decade, new photon sources became available and others are under construction [e.g., the Extreme Light Infrastructure - Nuclear Physics (ELI-NP) [19]]. In response to the growing needs for photonuclear data, IAEA-NDS initiated a research project on Photonuclear Data and Photon Strength Functions , with the primary task to create a new IAEA Photonuclear Data Library [20] as well as a database of photon-strength functions [21]. Several evaluations based on photoreaction calculations performed with the EMPIRE code have been already included in this library [20].

The calculated photoreaction cross sections for $^{233–238}$U which are in agreement with the experimental data, as well as the models (e.g., the extended optical model for fission) and the parameters (e.g., for the Giant Dipole Resonances and for the fission barriers) reported in this paper integrate into this context of scientific interest.

II. REACTION MODELS AND PARAMETERS

The models and parameters implemented in the EMPIRE-3.2 code [17] and used for the present photoreaction calculations on uranium isotopes are briefly outlined, mentioning the differences and the similarities with the models and parameters used in Ref. [2] for the calculations of neutron-induced

*r.capotenoy@iaea.org

reactions on the same target nuclei. Initial values of the model parameters are automatically retrieved in the EMPIRE code from the Reference Input Parameter Library (RIPL-3) [22].

A. Incident channel

The photonuclear excitation process is described by two mechanisms: the excitation of the isovector Giant Dipole Resonances (GDR) which dominates at low energies, below about 30 MeV, and the photo-absorption on a neutron-proton pair (a quasideuteron, QD) which dominates at higher energies.

The total gamma cross section is calculated in the EMPIRE code as the sum of two components [17,18],

$$\sigma_{\gamma t}(E_\gamma) = \sigma_{\rm GDR}(E_\gamma) + \sigma_{\rm QD}(E_\gamma). \quad (1)$$

The QD component $\sigma_{\rm QD}(E_\gamma)$ has a small contribution in the studied energy range and is not discussed in this paper. The GDR component, $\sigma_{\rm GDR}(E_\gamma)$, is calculated in terms of the photoexcitation (upward) strength function $\overrightarrow{f}$:

$$\sigma_{\rm GDR}(E_\gamma) = 3(\pi\hbar c)^2 E_\gamma \overrightarrow{f}(E_\gamma). \quad (2)$$

In RIPL-3 there are several Lorentzian-type closed-form expressions for the dipole radiative (downward) $\overleftarrow{f}$ and excitation (upward) $\overrightarrow{f}$ strength functions, as well as microscopic Hartree-Fock-Bogoliubov plus quasiparticle random-phase approximation model predictions for these quantities. Theoretical details about these formulations can be found in Ref. [22]. All of them are implemented in the EMPIRE code.

The phenomenological expression of the excitation strength function for the cold and deformed nuclei (in units of MeV^{-3}) is the sum of two Lorentzian shapes:

$$\overrightarrow{f}(E_\gamma) = c\sum_{i=1}^{2}\sigma_{ri}\Gamma_{ri}\frac{E_\gamma\Gamma_i(E_\gamma)}{\left(E_\gamma^2 - E_{ri}^2\right)^2 + [E_\gamma\Gamma_i(E_\gamma)]^2}, \quad (3)$$

where $c = 8.674\times10^{-8}$, and σ_{ri}, E_{ri}, and Γ_{ri} are the GDR peak cross section (in mb), energy and width (in MeV), respectively. The different closed-form expressions treat differently $\Gamma_i(E_\gamma)$, a quantity which takes into account the collective state damping. After testing all of them, in the EMPIRE code was selected as default option the Modified Lorentzian 1 (MLO1) strength function that involves the use of the Landau-Vlasov equation with a collision term. More on the calculation of $\Gamma_i(E_\gamma)$ in MLO1 approach can be found in Refs. [22–25].

If the excitation of the GDRs is considered the only (or the dominant) excitation mechanism, one assumes that only electric-dipole transitions or only photons with zero orbital momentum are involved. Because of the conservation laws which act as selection rules, the photoexcited compound nucleus is populated only in states with spins and parities $J = J_0 \pm 1$, $\pi = -\pi_0$, where J_0, π_0 are the spin and parity of the target in the ground state. In reality this is true only at low energies, because at higher energies, due to the gamma cascade, the compound nucleus can have different spins and parities. In the reactions induced by fast neutrons, which may have higher orbital momenta, such a strict selectivity in spin and parity does not appear.

B. Exit channels

According to the Bohr hypothesis [26], the compound nucleus should have decay probabilities independent of its formation. In photon- and neutron-induced reactions the compound nucleus is not populated in the same states, therefore the decay probabilities in the two cases are not expected to be the same, but it is expected to be described by the same models and parameters. This assumption was tested by using, for the present photoreaction calculations, the same models and parameters used in Ref. [2] to describe the outgoing channels in neutron induced reactions.

The main outgoing channels up to 30 MeV incident energy are gamma decay (γ,γ), neutron emission (γ,n), $(\gamma,2n)$, $(\gamma,3n)$ and fission (γ,f). The charged-particle emission (p, α, d, t, ^{3}He) become comparable with the neutron emission around 30 MeV, but have a small contribution below 20 MeV. Not being relevant for the aim of this paper, they are not further discussed but are considered in calculations as competing channels. The photon, neutron, and charged-particle emission have a pre-equilibrium and a compound nucleus component, while fission is a compound nucleus process.

Pre-equilibrium emission was described by the one-exciton model with gamma, nucleon, and cluster emissions implemented in the EMPIRE module PCROSS [27]. The Hauser-Feshbach model [28] with full gamma cascade and exact angular momentum and parity coupling was employed for the compound nucleus reaction calculations. It should be noted that width-fluctuation corrections do not play an important role for photon-induced reactions [29], nor the effects of deformation studied in Ref. [30]. The particle transmission coefficients have been calculated with the same optical potentials as in Ref. [2]. For the gamma transmission coefficients was used the MLO1 radiative strength function with GDR parameters obtained in this paper. The discrete levels for the compound nucleus and the residual nuclei were retrieved from RIPL-3. The level densities, both at the equilibrium deformation and at the saddle points, have been described with the enhanced generalized superfluid model (EGSM) and the same parameters as in Ref. [2].

The fission coefficients have been calculated with the extended optical model for fission (OMF). In OMF the main fission mode is associated with the nuclear vibrational motion, so that the key role is played by (i) the coupling between the vibrational states with similar excitation energies, the same spin projection on the symmetry axis and parity, which are located in different wells of the fission barrier, and (ii) by the coupling between the vibrational states in each well and other degrees of freedom which increases with increasing the excitation energy above the bottom of the well.

The first type of coupling is responsible for the direct resonant transmission across the multihumped barrier at the excitation energies of the vibrational states in the wells. The second type of coupling which dissipates or damps the vibrational strength of the states is interpreted as an absorption out of the fission mode and is simulated by adding, to the real part of the deformation potential, imaginary term(s) in the region of the well(s). This second type of coupling is responsible for the indirect transmission mechanism representing

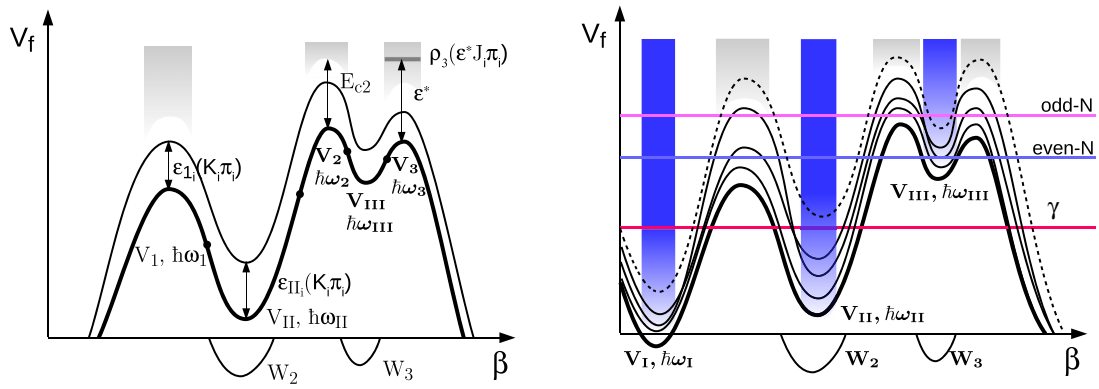

FIG. 1. Triple-humped fission barriers of light actinides (explanations provided in text).

transmission through the outer hump(s) after absorption in the well(s).

In the EMPIRE code it is implemented a very compact and elegant formulation of OMF which describes transmission through barriers with any number of humps and absorption in any number of wells [2,31,32].

In the present work have been considered, as in Ref. [2], triple-humped barriers for $^{231–237}$U (^{231,232}U are responsible for the second and third fission chances in ^{233}U(γ, f) reaction) and a double-humped barrier for ^{238}U. The model implemented in EMPIRE was applied before for the neutron-induced fission of light actinides with triple-humped barriers as ^{232}Th, ^{231,233}Pa [33], and $^{232–237}$U [2]. It is worth recalling that the evaluations performed based on the model calculations for ^{232}Th, ^{231,233}Pa, and ^{235,238}U were adopted by the ENDF/B-VIII.0 library [10], the evaluations for ^{235,238}U being included also in the CIELO library [8].

The OMF formalism and the parametrization of the fission barriers are fully described in Ref. [31] and rehashed in Ref. [2], therefore only selected features of interest for the present work are reviewed in this contribution.

In Fig. 1 it is sketched a typical triple-humped barrier for light actinides as a function of deformation β considered to have the inner hump (with height V_1 and curvature $\hbar\omega_1$) wider and lower than the outer humps (with heights V_2 and V_3, and corresponding curvatures $\hbar\omega_2$ and $\hbar\omega_3$). The second well with height $V_{\rm II}$ and curvature $\hbar\omega_{\rm II}$ which accommodates the superdeformed (class II) states is much deeper than the third well with height $V_{\rm III}$ and curvature $\hbar\omega_{\rm III}$ which accommodates the hyper-deformed (class III) states (the class I states are the normal states situated in the first well $V_{\rm I}$ corresponding to the equilibrium deformation which is only shown in the right panel of the figure). The bold black curve represents the fundamental barrier, with thinner black lines representing the barriers associated with the fission paths of the nucleus in different discrete excited states, and the continuum spectra of the transition states represented in gray shadows. The imaginary potentials W_2 and W_3 are introduced in the wells region to simulate the damping of the vibrational strength of the class II and III states. As exemplified in the left panel of Fig. 1, for barriers with parabolic representation the fission input parameters are (i) the heights $V_{\rm i}$ and curvatures or widths $\hbar\omega_{\rm i}$ of the humps/wells (i = 1, 2, 3/II,III) of the fundamental barrier, (ii) the sets $\varepsilon_{\rm i}(K\pi)$ representing the excitation energy of discrete levels with respect to the fundamental barrier at saddle points and in wells, the spin projection along the symmetry axis, and the parity, for each discrete barrier, (iii) the parameters defining the transition states densities $\rho_{\rm i}(\varepsilon^*, J, \pi)$, i = 1, 2, 3 for the continuum above the humps $V_{\rm i}$, and (iv) the strengths of the imaginary potentials W_2 and W_3. Note that the barrier continuity condition requires the same number of discrete levels in all wells and barriers.

In the right panel of Fig. 1 the gradients in blue suggest the vibrational strength's degree of damping for the class I, II, and III states. The horizontal lines indicate the excitation energy of the compound nucleus (CN) formed in three situations: after absorption of photons with incident energy of about 3 MeV (red line), after absorption of neutrons with incident energy of about 10 keV by an even-N fertile target (blue line) and by an odd-N fissile target (magenta line). The incident energies selected for this illustration are the lowest ones considered in the present work for photons and in Ref. [2] for neutrons. This picture reveals several aspects important for the fission modeling below the excitation energy of approximately 6–7 MeV: (i) at 3 MeV the class I vibrational states (in the minimum $V_{\rm I}$ corresponding to the equilibrium deformation) are already completely damped, therefore the first well is not included in the parametrization of the deformation potential shown in the left panel, (ii) the different shades of blue (degree of damping) in the second and third well at the three excitation energies taken as example explain the different behavior of the photon- and neutron-induced fission cross sections at low energies, as discussed in the next section, (iii) the dashed line barrier indicates that the class III vibrational states associated with barriers with maxima in the continuum still can be only partially damped, (iv) the full damping approximation implemented in most of the statistical reaction codes obviously cannot be used in this energy range.

Expressions relevant for photon-induced fission on nuclei with triple-humped barriers have been extracted from the extended OMF formalism and will be discussed below. In the left panel of Fig. 2 are represented the transmission mechanisms through a triple-humped fission barrier at the excitation energy E: the blue arrows represent forward and backward direct transmission through one or more humps, and the bent red arrows describe the absorption in the wells. The total

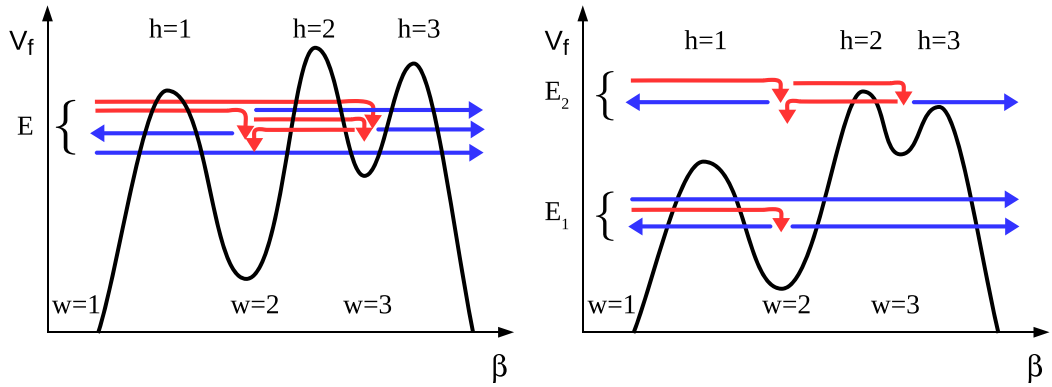

FIG. 2. Transmission mechanisms through triple-humped fission barriers (explanations provided in text).

fission coefficient is the sum of the direct transmission through the entire barrier ($T_d^{(1,3)}$) and two indirect terms representing re-emission in the fission channel after absorption in the second ($T_i^{(2)}$) and third well ($T_i^{(3)}$):

$$T_f = T_d^{(1,3)} + R\left[T_i^{(2)} + T_i^{(3)}\right]. \tag{4}$$

The normalization factor R, defined by Eq. (8), takes into account the infinite sequence of shape transitions of the nucleus between wells ensuring the flux conservation. The indirect transmission coefficients have the expressions

$$T_i^{(2)} = T_a^{(1,2)}\left[\frac{T_d^{(2,3)}}{\sum T(2)} + \frac{T_a^{(2,3)}}{\sum T(2)}\frac{T_3}{\sum T(3)}\right], \tag{5}$$

$$T_i^{(3)} = T_a^{(1,3)}\left[\frac{T_3}{\sum T(3)} + \frac{T_a^{(3,2)}}{\sum T(3)}\frac{T_d^{(2,3)}}{\sum T(2)}\right], \tag{6}$$

where $T_d^{(h,h')}$ represent the direct transmission coefficients through the humps $h \div h'$, $T_a^{(w,w')}$ represent the absorption coefficients from well w into well w', and T_h stands for the transmission through hump h ($T_h = T_d^{(h,h)}$). These transmission coefficients are calculated using the recursive procedure presented in Ref. [32], having as starting point the expressions for a double-humped barrier proposed by Bhandari in Ref. [34]. These expressions are derived in the first-order Jeffreys-Wentzel-Kramers-Brillouin (JWKB) approximation [35,36], in terms of momentum integrals for the humps and the wells of the real barrier and for the imaginary potential(s). The denominators in the above equations represent the sum of the transmission coefficients for the competing channels specific to the second and third wells,

$$\sum T(2) = T_1 + T_d^{(2,3)} + T_a^{(2,3)} + T_\gamma^{(2)},$$
$$\sum T(3) = T_d^{(2,1)} + T_3 + T_a^{(3,2)} + T_\gamma^{(3)}. \tag{7}$$

The gamma decay in the second and third wells has been considered in an approximate way, but the contribution of the isomeric (delayed) fission has been ignored. From a superdeformed state a shape isomer would decay mainly by gamma emission, while the fission of a hyper-deformed shape isomer would occur at energies higher than the third well (≈5 MeV) where the delayed fission contribution would be negligible. However, this subject needs further studies.

The normalization factor R reads

$$R = \left[1 - \frac{T_a^{(2,3)}}{\sum T(2)}\frac{T_a^{(3,2)}}{\sum T(3)}\right]^{-1}. \tag{8}$$

The right panel of Fig. 2 presents two particular situations: transmission at an excitation energy E_1 lower than the third well, and transmission at an excitation energy E_2 at which full-damping limit of the vibrational class II and III states is reached.

Below the third well the absorption coefficients $T_a^{(1,3)}$, $T_a^{(2,3)}$ are zero and Eq. (4) becomes an expression typical for the fission coefficient of a double-humped barrier

$$T_f = T_d^{(1,23)} + T_a^{(1,2)}\frac{T_d^{(23)}}{T_1 + T_d^{(23)} + T_\gamma^{(2)}}. \tag{9}$$

In the full-damping limit (which is equivalent to full flux absorption) corresponding to the excitation energy E_2, the direct transmissions through more than one hump disappear (consequently $T_a^{(1,3)} \to 0$), and the transmission across each hump is fully absorbed in the next well,

$$T_d^{(1,2)} \to 0, \quad T_d^{(1,3)} \to 0, \quad T_d^{(3,2)} \to 0,$$
$$T_a^{(1,2)} \to T_1, \quad T_a^{(2,3)} \to T_2, \quad T_a^{(3,2)} \to T_2. \tag{10}$$

As expected, Eq. (4) takes the classical form

$$T_f = \frac{T_1 T_2 T_3}{T_1 T_2 + T_1 T_3 + T_2 T_3}. \tag{11}$$

Another important aspect for the description of the fission cross section at excitation energies lower than 5–6 MeV is the treatment of the fission channels in the lower part of the continuum spectrum. Equations (4)–(11) refer to the transmission coefficients for a single barrier. However, the spin- and parity-dependent ($J\pi$-dependent) fission coefficients (which we call effective fission coefficients) enter the Hauser-Feshbach formula for the compound nucleus cross sections [28]. Those effective coefficients represent the transmission through all the barriers associated with the discrete and the continuous spectrum of the transition states with the same $J\pi$. Therefore, the single-hump transmission and the direct and absorption coefficients are the sum of two contributions corresponding to the discrete and to the continuous part of the transition

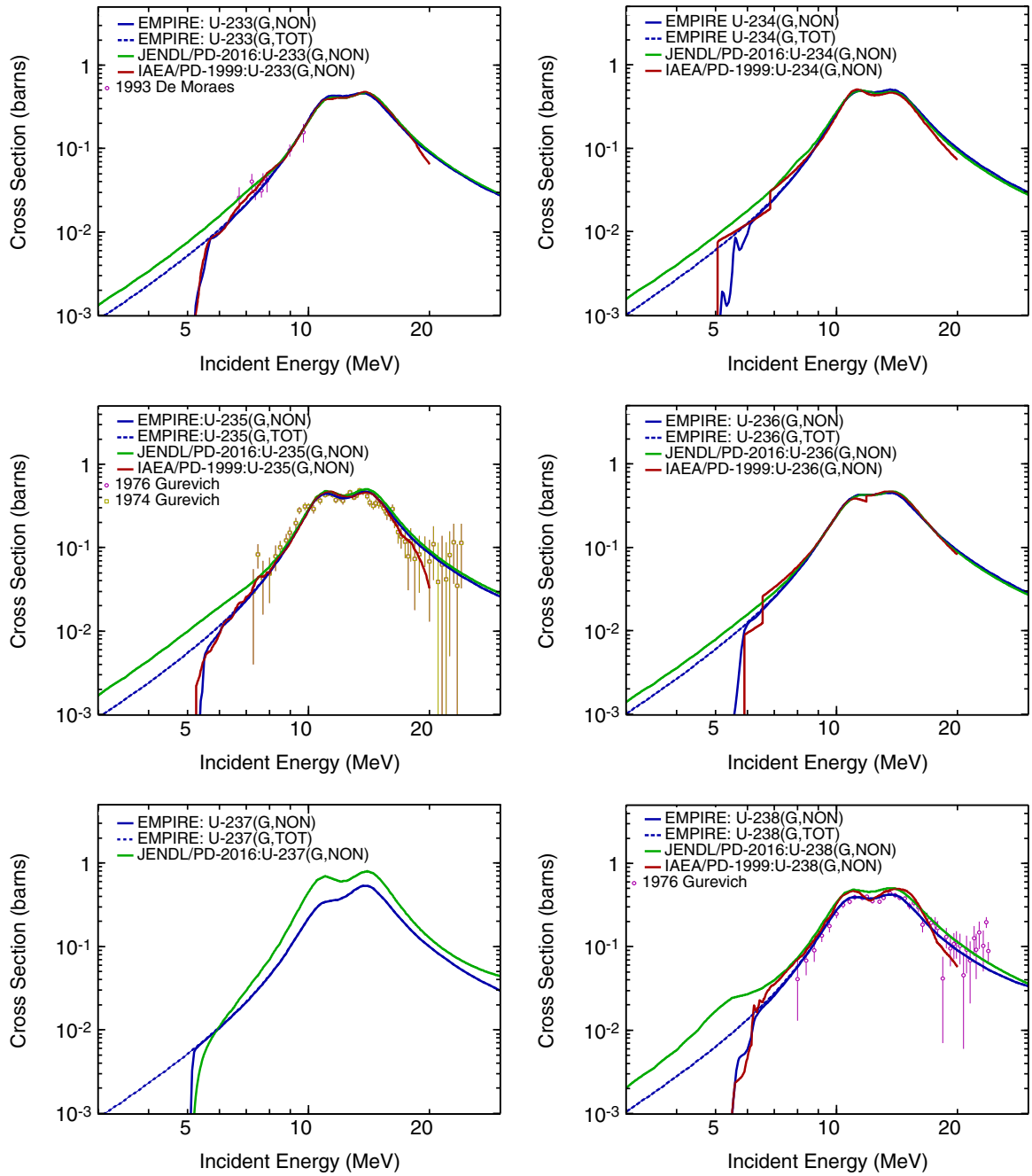

FIG. 3. JENDL-PD total cross section (green line), IAEA-PD nonelastic cross section (red line), calculated total (dashed blue line), and nonelastic (blue line) cross sections for $^{233-238}$U compared with experimental data from EXFOR [42,43]. Note that the photoinduced reactions (γ, non) and (γ, tot) are denoted in legend as (G, NON) and (G, TOT), correspondingly.

state spectrum. The calculation of these effective fission coefficients is presented in detail in Refs. [2,31]. In this paper only simplified expressions for the continuum contribution are reproduced in which the explicit dependence on energy, spin, and parity is omitted.

The continuum contribution to the transmission coefficient across the hump h is calculated as

$$T_{h,\mathrm{cont}} = \int_{E_{ch}}^{\infty} \frac{\rho_h(\varepsilon^*)d\varepsilon^*}{1+\exp\left[-\frac{2\pi}{\hbar\omega_h}(E-V_h-\varepsilon^*)\right]}, \qquad (12)$$

where V_h, $\hbar\omega_h$ are the parameters of the hump h of the fundamental barrier ($h = 1, 3$), ρ_h is the transition states density function, E is the excitation energy, and E_{ch} is the energy where continuum starts with respect to the top of hump h (see Fig. 1).

For a triple-humped barrier with a deep second well and a shallow third well the continuum contribution to different direct and absorption coefficients is different. The superdeformed (class II) vibrational states are completely damped at the energies where the transmission across the barriers in continuum becomes significant, so there is no direct trans-

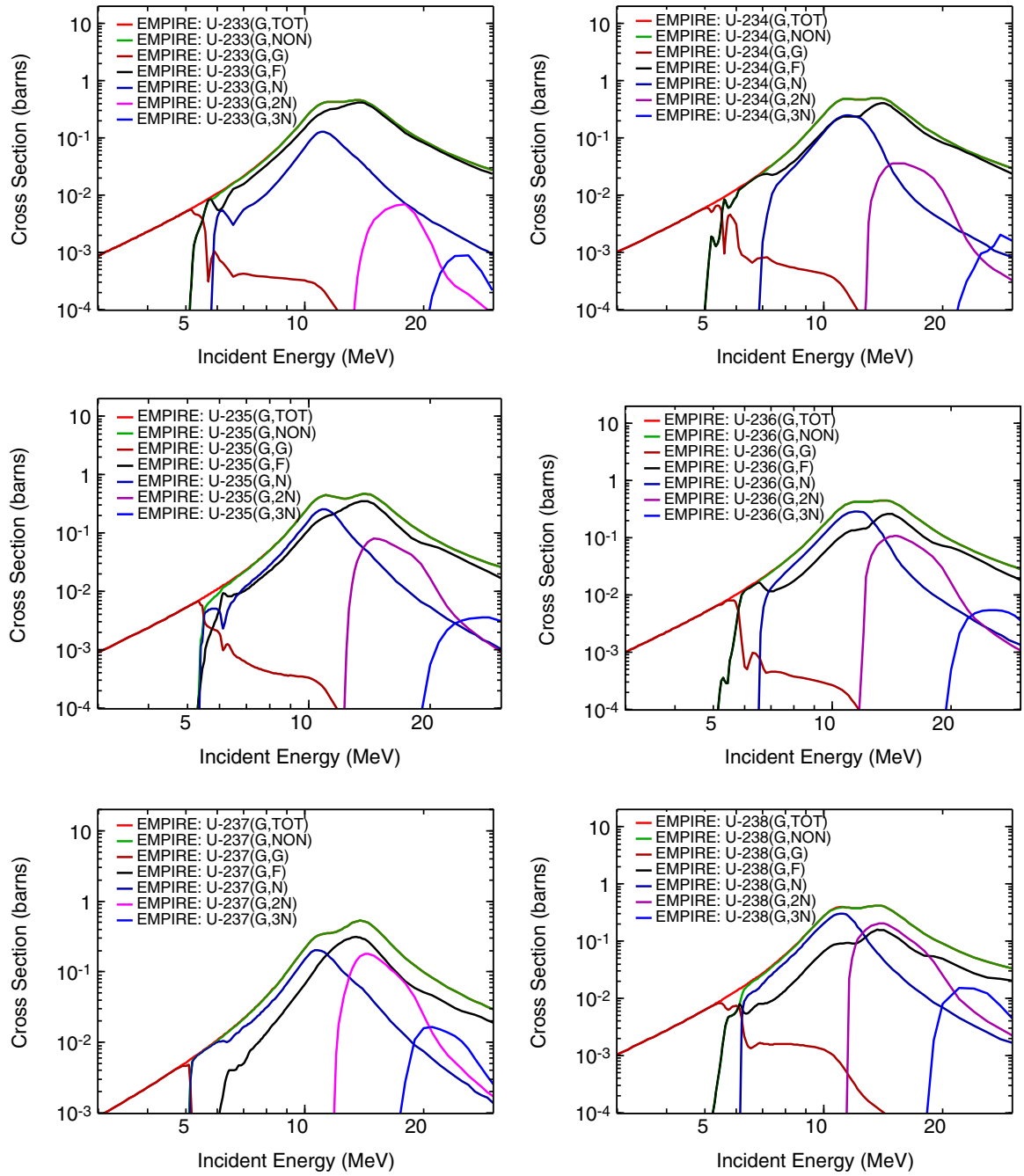

FIG. 4. Photoreaction cross sections for $^{233-238}$U calculated with EMPIRE code: total (light-red), photoabsorption (green), fission (black), (γ,γ) (red), (γ,n) (blue), $(\gamma,2n)$ (magenta), $(\gamma,3n)$ (light blue). Note that the photoreaction cross sections $(\gamma,...)$ are denoted in the legend as (G, ...), correspondingly.

mission via these states, only full absorption in the second well (obviously there is no direct transmission across an entire barrier in continuum),

$$T^{(1,2)}_{d,\mathrm{cont}} = 0, \quad T^{(3,2)}_{d,\mathrm{cont}} = 0, \quad T^{(1,3)}_{d,\mathrm{cont}} = 0,$$
$$T^{(1,2)}_{a,\mathrm{cont}} = T_{1,\mathrm{cont}}, \quad T^{(3,2)}_{a,\mathrm{cont}} = T_{2,\mathrm{cont}}.$$

On the other hand, the hyper-deformed vibrational states might not be fully damped at the excitation energies where the transmission through the barriers in continuum becomes important (see the dashed line barrier in the right panel of Fig. 1). As explained in Refs. [2,31], the treatment of partial damping for discrete barriers which cannot be applied for those in continuum is replaced by a surrogate for the optical model for fission [13,14,37]. In this approach, the degree of damping is simulated by using a linear combination of a direct transmission coefficient through the outer humps corresponding to the zero-damping limit, and an indirect transmission coefficient corresponding to the full damping of the class III vibrational states. The continuum contributions to the direct

and absorption coefficients involving the third well are

$$T^{(2,3)}_{\mathrm{dir,cont}} = (1-p_3)T^{(2,3)}_{d_{(0)},\mathrm{cont}},$$
$$T^{(2,3)}_{\mathrm{abs,cont}} = p_3 T^{(2,3)}_{a_{(f)},\mathrm{cont}}. \quad (13)$$

The expression for direct transmission coefficient corresponding to the zero-damping limit $T^{(2,3)}_{d_{(0)},\mathrm{cont}}$ is provided in Refs. [2,31], and $T^{(2,3)}_{a_{(f)},\mathrm{cont}} \rightarrow T_{2,\mathrm{cont}}$. The definition of the energy dependent weight p_3 given in Refs. [2,31] was changed to become valid at excitation energies lower than the third well and became

$$p_3 = \frac{E^2}{V_d^2 \exp[-(E-V_d)/b_3]}, \quad (14)$$

where V_d is the excitation energy where the full-damping limit is supposed to be reached and b_3 is a parameter which controls the energy dependence of the weight.

Considering the partial damping of the fission channels in the lower part of continuum represents the extension of the optical model for fission.

The impact of the optical model for fission and of its extended version on the photofission cross sections of odd- and even-N uranium isotopes is shown in Fig. 7 and commented in Sec. III C.

III. RESULTS AND DISCUSSIONS

The results of our calculations performed with the EMPIRE code for the photo-absorption, (γ, n), $(\gamma, 2n)$, and (γ, f) cross sections are compared with the available experimental data from the EXFOR library [38] and with the evaluated data from JENDL/PD-2016 (JENDL-PD) [39] and IAEA-Photonuclear Data Library 1999 (IAEA-PD) [40].

To explain some of the similarities and differences between EMPIRE calculations and evaluations, it is worth mentioning that JENDL-PD relies mainly on model calculations performed with the CCONE code [12] (which in many respects is close to EMPIRE code [41]), while IAEA-PD is mostly based on least-squares fit of the experimental data.

A. Photoabsorption cross sections

The photoabsorption cross section is defined as the difference between the total gamma cross section (1) and the elastic scattered gamma $\sigma_{\gamma\gamma}$ cross section:

$$\sigma_{\mathrm{abs}}(E_\gamma) = \sigma_{\gamma t}(E_\gamma) - \sigma_{\gamma\gamma}(E_\gamma). \quad (15)$$

Generally, the reaction evaluated data libraries include the photoabsorption as a nonelastic cross section and do not include the total gamma cross section [44]. In IAEA-PD this formatting rule is applied, but in JENDL-PD it is assumed that the nonelastic is equal to the total gamma cross section (except for ^{237}U). Therefore, in Fig. 3 both total gamma and photoabsorption calculated cross sections are presented for comparison. From Fig. 4 one can notice that the total gamma cross section (light-red line) is visible only in a small energy range around the fission threshold, being overwritten at lower energies by the gamma emission cross section and by the nonelastic cross section at higher energies.

For photon-induced reactions, the total gamma and photoabsorption cross-section calculation requires GDR parameters, see Eqs. (1)–(3), the same way the optical potentials are needed for the total cross-section calculation in the particle-induced reactions. For particle-induced reactions, in particular for neutrons, the global or regional optical potentials are usually quite reliable, providing accurate total cross sections, as well as a proper partition between direct elastic and nonelastic cross sections. For photon-induced reactions on actinides there is not enough experimental information for a reliable parametrization of the GDR parameters [24,25], and the available microscopic strength functions (e.g., from Refs. [21,45]) are useful to set trends but the normalization is typically more uncertain as judged by comparison with those cases where experimental data are available. Therefore, if in the neutron-induced reactions the nonelastic cross section provided by optical model calculations has to be distributed in the outgoing channels, for those photon-induced reactions where no experimental photoabsorption data are available, the order is somehow reversed: the GDR parameters are adjusted to produce a nonelastic cross section equal to the sum of the cross sections for the open channels which fit the corresponding experimental data. The GDR parameters used in this paper and presented in Table I have been obtained by adjusting the RIPL-3 "experimental" parameters (derived as explained above) to improve the description of the experimental data.

TABLE I. GDR parameters for $^{233-238}$U used in the present work.

CN	E_{γ_1} (MeV)	Γ_{γ_1} (MeV)	σ_{γ_1} (mb)	E_{γ_2} (MeV)	Γ_{γ_2} (MeV)	σ_{γ_2} (mb)
^{233}U	11.3	3.0	320.0	14.0	4.3	360
^{234}U	11.2	3.2	370.0	14.1	4.3	380
^{235}U	11.0	2.8	370.0	14.1	4.0	380
^{236}U	11.3	3.4	320.0	14.0	4.5	320
^{237}U	11.2	3.2	360.0	14.0	4.3	380
^{238}U	11.0	3.3	316.0	14.1	4.4	320

Figure 3 shows that our calculations agree well with the experimental data, and that there are not significant differences between our calculations and the two evaluations around the GDR energies, except for ^{237}U. The behavior at low energies (underestimation of the JENDL-PD total gamma cross section and the agreement with the IAEA-PD nonelastic cross section) is related mainly to the description of the fission cross section, as can be seen in Fig. 8. The lower values of the IAEA-PD nonelastic cross section at higher energies are reflected in the corresponding values of the fission and $(\gamma, 2n)$ cross sections.

^{237}U is different from the other isotopes for several reasons: (i) no experimental information is available, (ii) there is no IAEA-PD evaluation, (iii) the JENDL-PD evaluation is based on other codes than the CCONE used for the rest of the isotopes and provides the photo-absorption cross section as nonelastic. Figure 3 shows a big difference ($\tilde{4}0\%$) between EMPIRE and JENDL-PD absorption cross sections, confirming that without experimental constraint, the model predictions can be very discrepant.

Small differences between JENDL-PD and IAEA-PD evaluations on one side and EMPIRE calculation and Gurevich

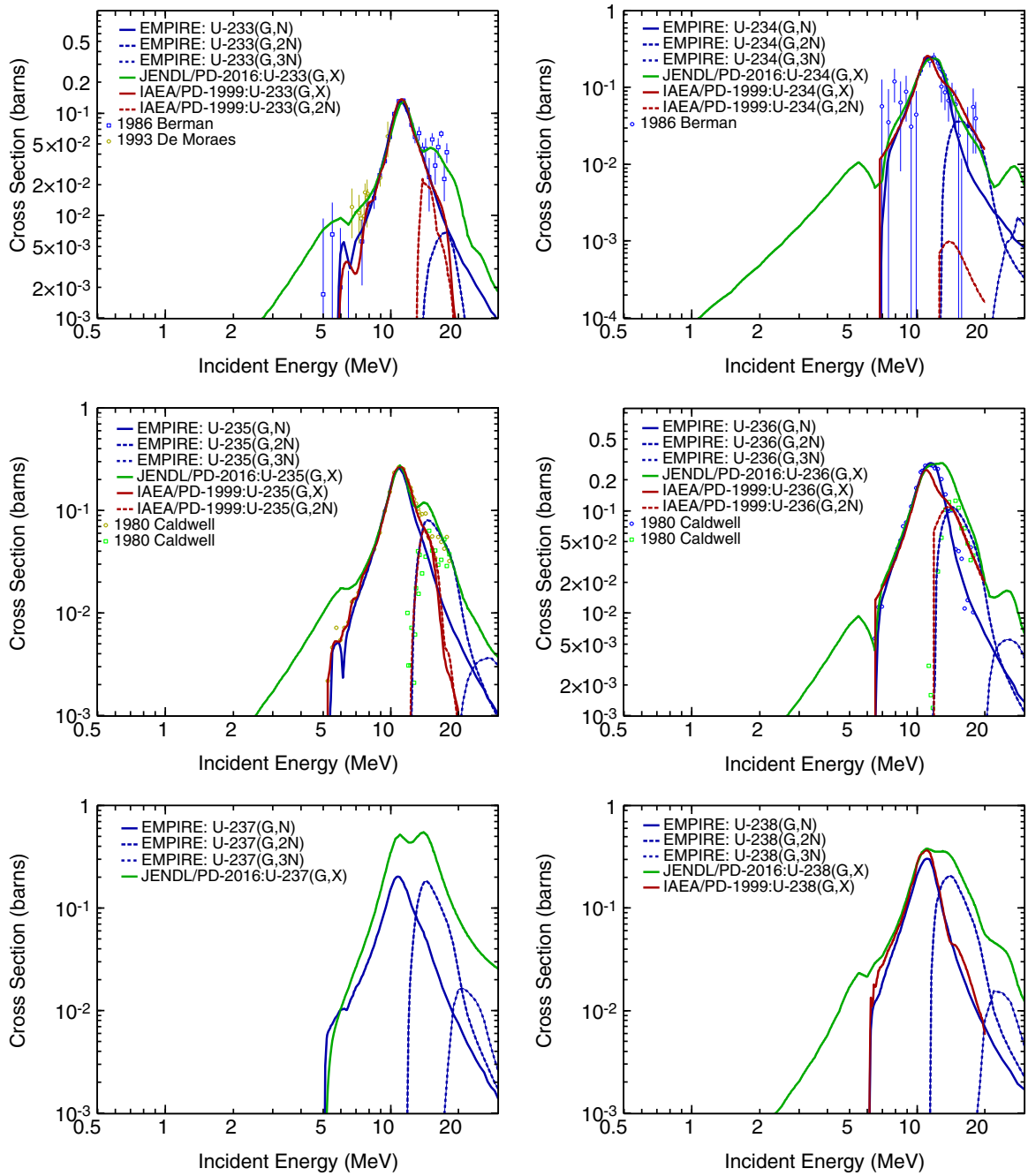

FIG. 5. Calculated neutron-emission cross sections [(γ, n) blue solid line, $(\gamma, 2n)$ blue dashed line, $(\gamma, 3n)$ blue dotted line] for $^{233-238}$U compared with evaluated (G, X) cross sections (JENDL-PD green line, IAEA-PD red line) and the experimental data from EXFOR [42,46,47]. Note that the neutron-emission cross sections $(\gamma, ...)$ are denoted in the legend as (G, ...).

experimental data [43] on the other side appear for ^{238}U also. The main reason is that the evaluations and our calculations describe different sets of experimental data for the (γ, f), (γ, n), and $(\gamma, 2n)$ processes, as discussed in the next sections.

B. Neutron-emission cross sections

The decay probabilities are constrained by the consistency of the preequilibrium and compound nucleus models and by the input parameters (optical potentials, discrete level schemes, level densities, fission parameters). The absolute values of the cross sections can be scaled by adjusting the GDR parameters. As pointed out in Sec. II, the decay of the photoexcited nuclei is treated with the same models and parameters used in Ref. [2] for the decay of the compound systems formed in neutron-induced reactions.

The EMPIRE neutron-emission cross sections are compared in Figs. 5 and 6 with JENDL-PD and IAEA-PD evaluations and with the experimental data from EXFOR. The signifi-

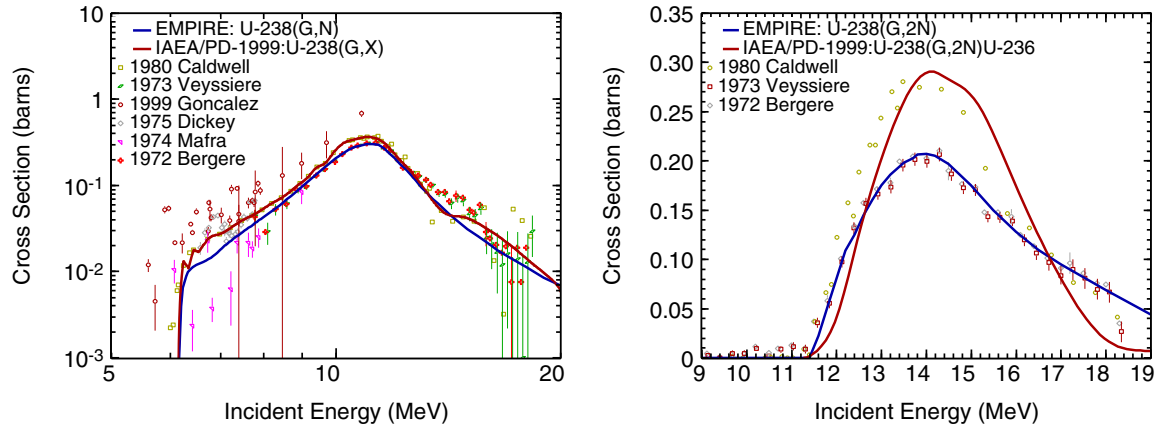

FIG. 6. IAEA-PD evaluation (red line) and EMPIRE calculation (blue line) for ^{238}U(γ, n) (left panel) and ^{238}U$(\gamma, 2n)$ (right panel) compared with experimental data from EXFOR [47–52]. Note that the (γ, n) and $(\gamma, 2n)$ cross sections are denoted in the legend as (G,N) and (G,2N), correspondingly.

cance of the evaluated curves and of the experimental data from these figures is clarified in the next paragraphs.

Most of the EXFOR data are presented as the sum $(\gamma, n) + (\gamma, np)$ cross sections, but, according to calculations, the second contribution can be neglected. However, the high values above the $(\gamma, 2n)$ threshold would suggest that the experimental data include multiple neutron emission also. Considering these aspects, the EMPIRE neutron-emission cross sections of $^{233–236}$U isotopes are in good agreement with the experimental data. An exception is the ^{235}U$(\gamma, 2n)$ which overestimates the experimental data of Caldwell [47].

JENDL-PD contains evaluations for the nonelastic (in reality total gamma) and fission cross sections, and a lumped cross section for the other channels: (γ, γ), (γ, n), $(\gamma, 2n)$, and $(\gamma, 3n)$. This lumped cross section symbolized as (G, X) is represented in Figs. 5 and 6. One can identify in these cross sections the high tail at low energies as the (γ, γ) contribution and the bumps at higher energies as produced by the $(\gamma, 2n)$, and $(\gamma, 3n)$ channels. For $^{233–236}$U isotopes the EMPIRE neutron-emission cross section is in good agreement with JENDL-PD evaluation around the maximum.

IAEA-PD includes an explicit evaluation for the $(\gamma, 2n)$ cross section but ignores the (γ, γ) and $(\gamma, 3n)$ contributions, so that the (G, X) evaluation represents in fact the (γ, n) cross section. The calculated (γ, n) cross section is in good agreement with IAEA-PD evaluation for ^{233}U, while for $^{234–236}$U isotopes, the agreement stops around 10 MeV incident energy. The differences between EMPIRE calculation and IAEA-PD evaluation above 10 MeV for the (γ, n) cross sections are reflected also in the $(\gamma, 2n)$ cross section, where they become even larger, especially for ^{234}U.

In the case of ^{237}U, the significant discrepancy between the calculated photoabsorption cross section and JENDL-PD evaluation is also reflected in the neutron-emission cross sections, as depicted in Fig. 5.

The same is true for ^{238}U of which the (γ, n) and $(\gamma, 2n)$ cross sections are plotted also separately in Fig. 6 with the corresponding experimental data. Using the parameters from

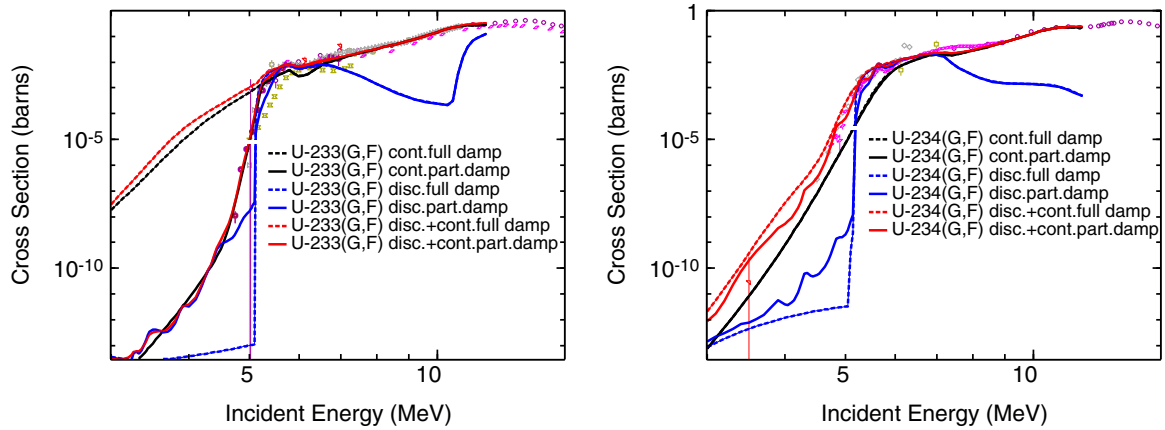

FIG. 7. The effect of considering different degrees of damping of the class III vibrational states corresponding to discrete fission barriers and to barriers in the lower limit of continuum on the fission cross section of ^{233,234}U. Fission cross sections (red line), the contributions of the discrete fission channels (blue line) and of the channels in continuum (black line), considering partial (solid line) and full (dashed line). Note that the (γ, f) cross sections are denoted in legend as (G,F).

TABLE II. Fission barrier parameters for description of neutron and photon-induced reactions on uranium isotopes. $V_1(\hbar\omega_1)$, $V_2(\hbar\omega_2)$, and $V_3(\hbar\omega_3)$ are the fission barrier heights (curvatures). $V_{II}(\hbar\omega_{II})$, $V_{III}(\hbar\omega_{III})$ are the second and third well heights (curvatures).

CN	V_1 (MeV)	$\hbar\omega_1$ (MeV)	V_{II} (MeV)	$\hbar\omega_{II}$ (MeV)	V_2 (MeV)	$\hbar\omega_2$ (MeV)	V_{III} (MeV)	$\hbar\omega_{III}$ (MeV)	V_3 (MeV)	$\hbar\omega_3$ (MeV)	Reaction
^{233}U	4.70	0.70	1.70	1.00	5.85	1.30	5.00	1.00	5.80	1.30	^{233}U(γ, f)
^{233}U	4.70	0.70	1.70	1.00	5.70	1.30	5.05	1.00	5.70	1.30	^{232}U(n, f)
^{234}U	4.70	0.60	1.70	1.00	5.83	1.40	5.00	1.00	5.83	1.40	^{234}U(γ, f)
^{234}U	4.60	0.60	1.60	1.00	5.90	1.30	5.20	1.00	5.70	1.30	^{233}U(n, f)
^{235}U	4.90	0.60	1.75	1.00	6.20	1.45	5.18	1.00	5.90	1.45	^{235}U(γ, f)
^{235}U	4.80	0.60	1.60	1.00	6.10	1.45	5.20	1.00	5.78	1.45	^{234}U(n, f)
^{236}U	5.10	0.60	1.60	1.00	5.87	1.45	4.90	1.00	5.65	1.45	^{236}U(γ, f)
^{236}U	4.60	0.60	1.60	1.00	5.90	1.45	4.90	1.00	5.64	1.45	^{235}U(n, f)
^{237}U	5.10	0.60	1.60	1.00	5.90	1.45	4.88	1.00	5.73	1.45	^{237}U(γ, f)
^{237}U	5.25	0.50	2.30	1.00	6.18	1.50	5.57	1.00	5.80	1.50	^{236}U(n, f)
^{238}U	6.15	1.00	1.60	1.00	5.50	0.60					^{238}U(γ, f)
^{238}U	6.30	1.00	1.60	1.00	5.50	0.60					^{237}U(n, f)

Ref. [2] and the GDR parameters from Table I, a simultaneous accurate description of the Veyssiere [48] and Bergere [49] data for the neutron-emission (Fig. 6) and fission (Fig. 8) cross sections has been obtained, but also of the Gurevich photoabsorption data [43] (Fig. 3). Impressive is the perfect fit of the $(\gamma, 2n)$ cross section. On the other hand, both evaluations follow the Caldwell data [47] and overestimate the experimental photoabsorption cross section. Caldwell data [47] are measured at Lawrence Livermore National Laboratory while Veyssiere [48] and Bergere [49] data are measured at CEA-Saclay Nuclear Research Center. There is a controversy in the literature regarding the experimental data measured by the Livermore and Saclay groups. There is not sufficient information to conclude that our model calculations support the data of one of these groups, but for ^{238}U, the Saclay data seem to be more consistent.

C. Fission cross sections

The main purpose of the present calculations is to describe photofission cross sections using the optical model for fission and to check the compatibility of the fission barriers deduced from the fit of the neutron-induced fission cross sections of uranium isotopes in Ref. [2] with the input parameters specific to photoreaction model calculations.

When judging how well the fission parameters from Ref. [2] describe the photon-induced fission cross sections one has to consider at least two specific features of the photoexcited compound nuclei: the access to lower excitation energies (due to the lack of photon separation energy), and the selectivity in spin and parity.

In Fig. 7 is presented the impact of the class II and III vibrational states' damping on the fission cross sections of ^{233}U (representative for the odd-A isotopes), and ^{234}U (representative for the even-even isotopes). This figure reveals the striking behavior of the contributions of the discrete and continuum fission channels corresponding to partial and full vibrational strength damping at excitation energies not reachable in the neutron-induced reactions. The first thing to notice is the different weight of the fission channels in continuum for the two types of nuclei at low energies. The explanation is that, for the odd-N nuclei, the continuum starts at lower excitation energies and the level densities are higher than in the even-even nuclei. A similar behavior was observed in the neutron-induced fission, as shown in Ref. [31] for ^{235}U and ^{236}U fissioning nuclei.[1] For the odd-A nuclei it is impossible to describe the fission cross section below and above the "threshold" with the same parameters of the triple-humped barrier without considering partial damping of the class III vibrational states associated with barriers with maxima in the lower part of the continuum spectrum. Interesting is also the contribution of the transmission through the discrete barriers at excitation energies lower than the third well, especially the role of the resonant direct transmission at energies corresponding to the class II vibrational states partially damped.

In Table II the parameters of the fundamental fission barrier used in the present calculations are compared with those from Ref. [2]. The heights of the first (lowest) hump V_1 are within 150 keV (which is the lowest possible fission barrier uncertainty estimated by mass models), excepting ^{236}U where a too large difference of 500 keV is listed, which certainly deserves further studies. The new values generally show a slight increase with increasing the mass number. Even if no information on the wells could be extracted from the neutron-induced reactions [2], the values adopted based on educated guesses are generally confirmed by the present calculations (excepting the previous out-of-range values—2.30 and 5.57 MeV—for the second and third wells in ^{237}U). The heights of the outer humps V_3 are also within 150 keV. Probably the most important confirmation is the value around 5 MeV for the bottom of the third well V_{III}. Note that fission cross-section calculations for neutron-induced reactions on even-even targets are very sensitive to the highest of the barriers, on odd-A targets usually the sensitivity is lower. Differences observed for second and third wells of ^{237}U deserve further investigation of the neutron-induced fission on ^{236}U.

[1] A less severe effect because of the higher excitation energies in (n, f) reactions.

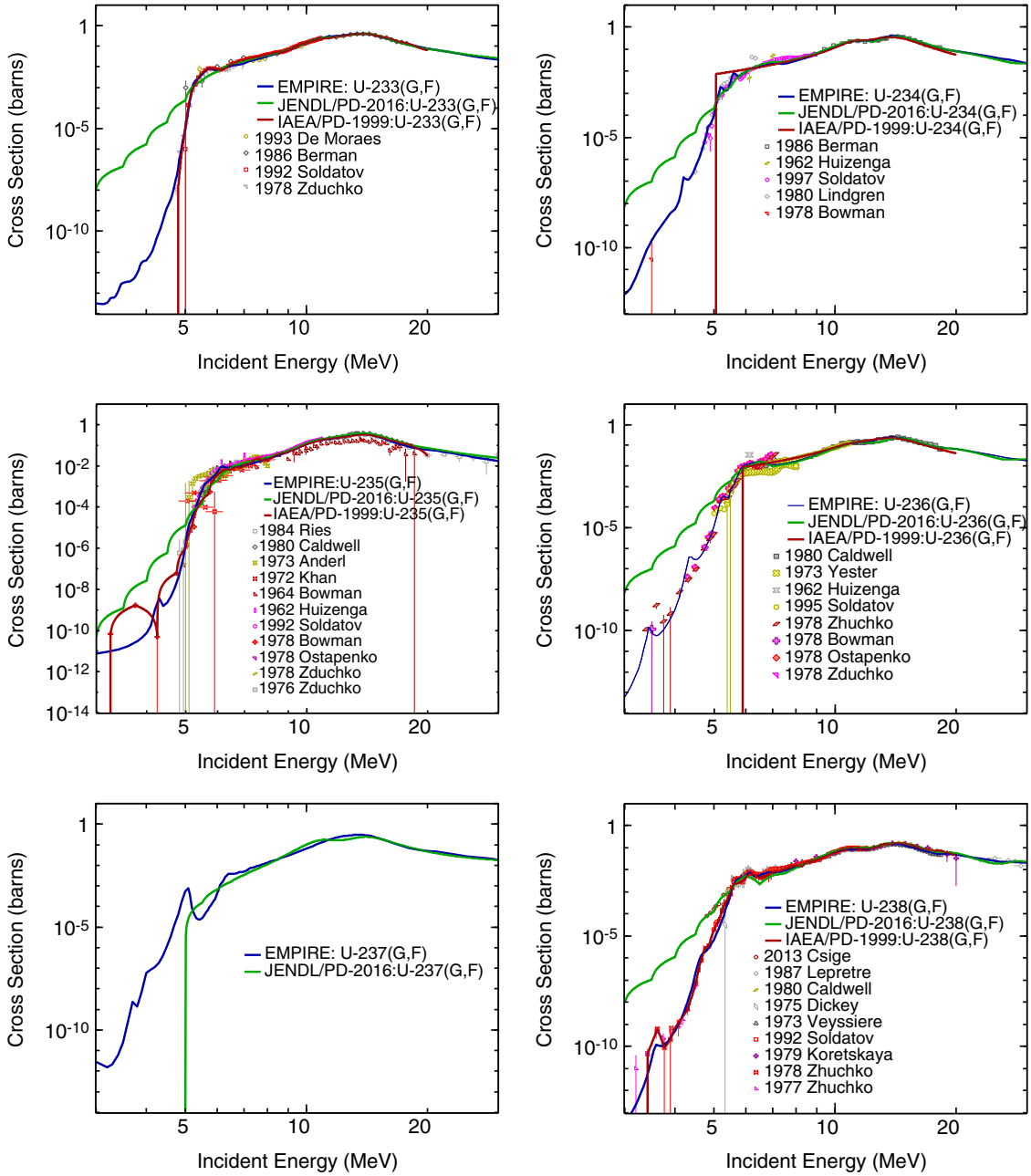

FIG. 8. EMPIRE calculations (blue line) and JENDL-PD (green line), IAEA-PD (red line) evaluations for the photofission cross sections of $^{233-238}$U compared with experimental data from EXFOR [42,46–49,51–76]. Note that the (γ, f) cross sections are denoted in the legend as (G,F).

For a fair and realistic analysis one should remind the reader that the role of the fundamental barrier is affected by the selectivity in spin and parity. In fact the barrier values in ^{236}U CN may show the effect of spin-population differences between neutron- and photon-induced reactions as the target ground-state spin of ^{235}U is 7/2 (the highest of uranium long-lived isotopes) vs the target ground-state spin of 0 for ^{236}U. If not known otherwise, to the fundamental barrier it is assigned the spin projection and parity equal to the spin and parity of the ground state of the fissioning nucleus. Considering the spins and parities of the target nuclei, of the neutron and of the photon, it is obvious that, by GDR photoexcitation, the nuclei will never be populated in states of spin and parity which belong to the fundamental rotational band, while the compound nuclei formed by absorption of neutrons (which may carry higher orbital momenta) can. In other words, the transmission through the fundamental barrier and through the barriers associated with the rotational band built on it, which represent a significant contribution to the neutron-induced fission cross section at low energies, is practically forbidden in photofission.

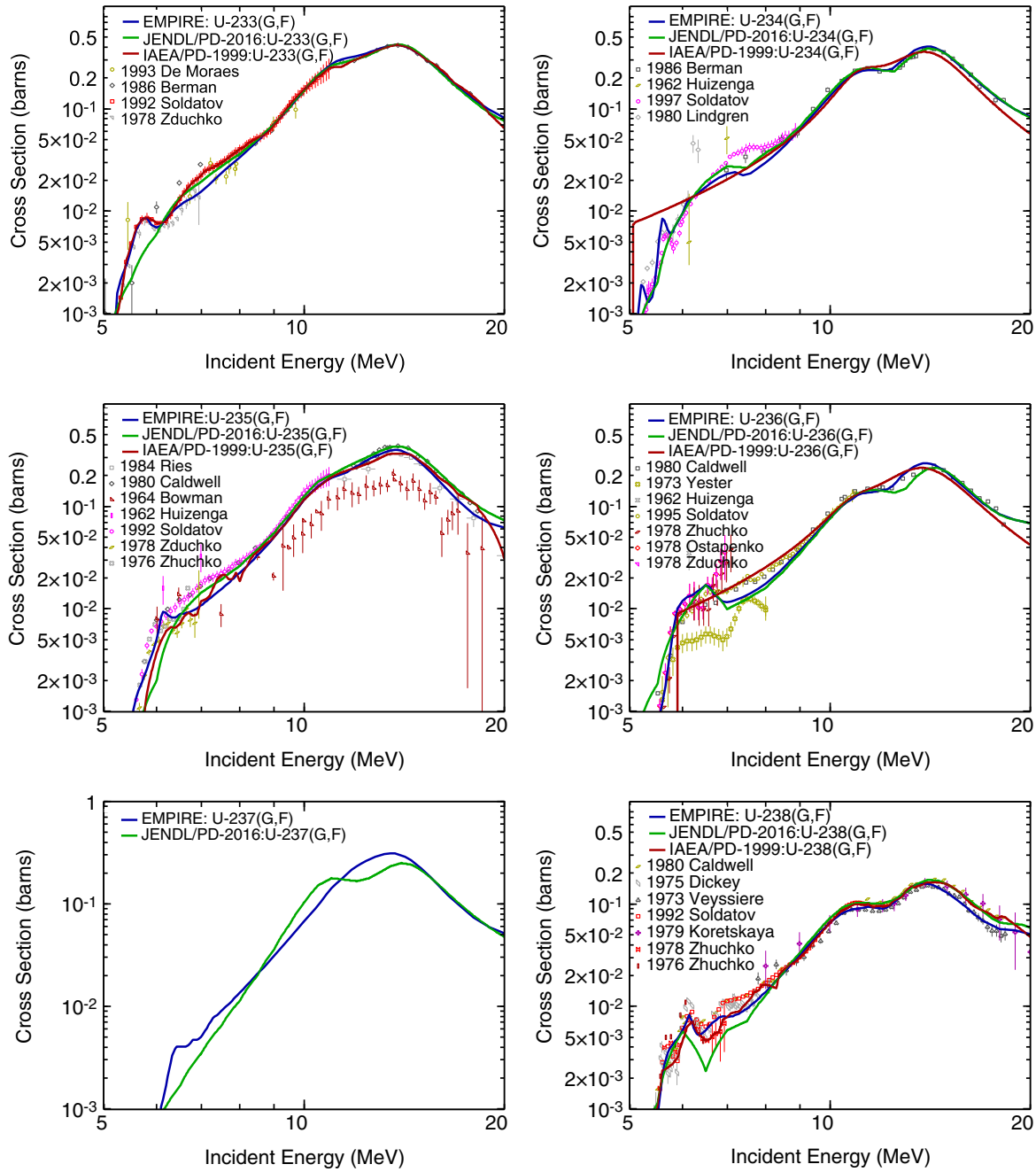

FIG. 9. EMPIRE calculations (blue line) and JENDL-PD (green line), IAEA-PD (red line) evaluations for the photofission cross sections of $^{233-238}$U in the incident energy range 5–20 MeV compared with experimental data from EXFOR [42,46–49,51,52,54–76]. Note that the (γ, f) cross sections are denoted in the legend as (G,F).

For example, for the even-even isotopes ^{234,236}U which are populated in states with $J^\pi = 1^-$, the transmission through the discrete barriers is determined by the absolute excitation energies of the rotational bandheads $K^\pi = 0^-, 1^-$ and less by the parameters of the fundamental barrier which has $K^\pi = 0^+$.

However, the heights and widths of the fundamental humps enter together with the level-density functions in the calculation of the transmission coefficients through the barriers in the continuum spectrum [Eq. (12)]. So, the role of the fundamental barrier remains very important for photofission also, especially at higher excitation energies, where the fission channels in continuum make the dominant contribution. Considering that the parameters of the level densities at saddles used in the present work are those from Ref. [2] adjusted in the limit of 5%, the agreement of the calculated photofission cross sections with the experimental data above 7 MeV represents a real test of the fundamental barrier parameters.

The most uncertain fission parameters are those of the discrete transition states, especially for the odd-A nuclei. For even-even nuclei, there are collective states within the pairing gap with $K^\pi = 0^+, 2^+, 0^-, 1^-$ and with excitation energies at the saddle points correlated with the nuclear shape asym-

metry at the corresponding deformations. But in general, if no other information are available, the sets $(\varepsilon, K\pi)$ are chosen to fit the experimental fission cross section.

The results of EMPIRE calculations are presented in Figs. 8 and 9 together with JENDL-PD and IAEA-PD evaluations and the experimental data from EXFOR. Once again, one can notice that JENDL-PD is based on model calculations. The shape of the JENDL-PD fission cross section at low energies indicates the use of a double-humped fission barrier in the full damping limit of the class II vibrational states. This is the reason why JENDL-PD fission cross sections overestimate the experimental data at those energies. IAEA-PD on the other hand, is based mainly on a nonmodel fit of the experimental data, the most evident example being ^{235}U case.

The experimental data for $^{233–236}$U(γ, f) cross sections are too scarce below 5 MeV to reveal a clear resonance structure. Still, for the even-even isotopes, for which the distance among the class II vibrational states is higher, hence their damping is lower, one can notice a resonance around 4.8 MeV for ^{234}U and a sequence of three resonances around 3.4, 4.3, and 5.3 MeV showed by the ^{236}U(γ, f) cross section. These resonances are not sharp enough to be generated by the class III vibrational states, therefore one can confirm that the energy associated with the bottom of the third well should be around 5 MeV. The opening of the fission channel, the absolute value and the slope of the fission cross sections, the damping of the resonance, and the distance between them have been used to extract information on the first hump and on the second well. This information is not available in neutron-induced reactions where the fission barrier cannot be explored at such low excitation energies.

In the energy range 5–8 MeV there are more experimental data, but the discrepancies among the different sets are significant. As shown in Fig. 4, there is an abrupt behavior of three cross sections in this range: gamma emission drops while fission and neutron emission rise. Therefore, the interpretation of the experimental fission cross section (Figs. 8 and 9) must consider the behavior of all cross sections shown in Fig. 4 because what seems to be threshold or resonance might be a structure generated by other causes.

The neutron separation energy decreases while nuclei become neutron richer, but has also a strong odd-even effect, so that for ^{233}U, ^{234}U, and ^{236}U there is an energy interval between the opening of the fission and of the neutron-emission channels. As gamma emission falls quickly once fission channel opens, in this energy interval fission remains the dominant decay and the photoabsorption and fission cross sections become almost equal (see Fig. 4). So, what looks at the first glance as a threshold is in fact a limitation imposed by the photoabsorption cross section and it is not directly related to the height of the fission barrier.

The neutron-induced fission cross sections of even-N light actinide targets (e.g., ^{232}Th, ^{231}Pa, ^{234,236}U) show in the same excitation energy range (5–8 MeV) a very clear resonance structure attributed to the low-damped class III vibrational states [2,33]. There are no similar resonances in the photofission cross sections, excepting ^{234}U, which has such a resonance around 5.6 MeV. More studies are needed to understand if this different behavior is related to experimental limitations or has other causes. The photofission cross sections of ^{233}U and ^{238}U have also maxima around 5.6 and 6.1 MeV respectively, which can be mistaken as resonances. In fact the resonant-like shapes are the effect of the dips around 6 and 6.6 MeV, respectively, caused by the opening of the neutron-emission channel. The calculated photofission cross sections of all isotopes have such a decrease, which does not appear to the same extent in the experimental data. One can notice the similar behavior in this region of the EMPIRE calculations and the JENDL-PD evaluations of ^{234,236}U(γ, f) cross sections.

At these energies (5–8 MeV) the calculated fission cross sections are most sensitive to the excitation energies of the discrete transition states, especially at the second and third saddle points, but also to the density of the transition states in continuum.

In the energy range 8–12 MeV the fission channels in continuum are the dominant contribution. Those fission channels are described by the EGSM level densities for the first fission chance. Depending on the neutron separation energies, the second and third fission chances open around 6 and 12 MeV and become significant around 13 and 20 MeV respectively. For the first and second residual nuclei the same fission parameters from Table II have been used. Our calculations agree well with the experimental data, and with the JENDL-PD evaluation in this energy range, excepting the already-discussed cases of ^{237}U and ^{238}U.

IV. CONCLUSIONS

Photoreaction cross-section calculations for the uranium isotopes have been performed with the EMPIRE-3.2 code in the energy range 3–30 MeV. The results give a comprehensive and systematic description of the photoreaction experimental data better than in existing evaluations. A set of GDR parameters consistent with all available experimental data are provided.

Except for the incident photon channel, the same reaction models for the neutron-induced reaction calculations in Ref. [2] have been used. The extended optical model for fission proved again to describe accurately the experimental fission cross sections at excitation energies below 7 MeV, in this case for photon-induced reactions.

The parameters of the fundamental triple-humped fission barriers derived from the analysis of the neutron-induced reactions on the uranium isotopes are close to those used in the current work for photon-induced reactions, with the exception of the inner barrier height of ^{236}U and well heights of ^{237}U. Most fission barriers and well heights for neutron- and photon-induced reactions agree within 150 keV, which is about the estimated potential-energy uncertainty from the best mass-model calculations. The inner V_1 (lowest) fission barrier of ^{236}U is estimated to be 500 keV higher for photon-induced reactions.[2] Relatively large differences were also observed for ^{237}U well heights. Unfortunately, lower fission barrier

[2]Such differences may drastically reduce the fission transmission of the inner barrier in the (n, f) description and result in relatively large deviations from experimental data at low incident neutron energies.

and well heights are very poorly constrained by cross-section calculations in neutron-induced reactions for fissile targets, as discussed in Ref. [2]. Target-spin and associated CN-spin differences for photon- and neutron-induced reactions may also impact derived barrier heights, especially for ^{236}U reactions. Further studies of these inconsistencies are needed.

The required barrier adjustment causing differences in the fission parameters sets has been expected considering (i) the different treatment of the entry channel, (ii) the specific and different sensitivity of the neutron- and photon-induced fission cross sections to fission parameters, and (iii) the model imperfections. Both fission parameter sets describing neutron- and photon-induced reactions are subjects for improvement. A future work to reconcile these differences is required in order to obtain a single fission parameter set which describes simultaneously the experimental data for both neutron- and photon-induced reaction cross sections. The access to low excitation energies allowed us to narrow the uncertainties of the first hump and second well fission parameters, and also confirmed the shallowness of the third well of which the energy of the bottom of the well is around 5 MeV.

This type of theoretical study which involves reactions induced by different projectiles leading to the same compound systems can identify data discrepancies, improve the models, and reduce the uncertainties of the model input parameters, and thus enhance the accuracy of the nuclear reaction data.

ACKNOWLEDGMENTS

The work of M.S. was partially supported by the IAEA under CRP F41033 Contract No. 20364, and UEFISCDI under PCE-2016-0014 Contract No. 7/2017. B.V.C. acknowledges support from Grant No. 2017/05660-0 of the Sao Paulo Research Foundation (FAPESP), grant 306433/2017-6 of the CNPq and the INCT-FNA Project No. 464898/2014-5. M.W.H. acknowledges support from the National Nuclear Security Administration of the US Department of Energy at Los Alamos National Laboratory under Contract No. 89233218CNA000001.

[1] R. Capote Noy, S. Goriely, S. Hilaire, O. Iwamoto, T. Kawano, A. Koning, and S. Simakov, Consultants' Meeting on Recommended Input Parameters for Fission Cross Section Calculation, 17–18 December 2013, Report IAEA(NDS)-0654 (International Atomic Energy Agency, Vienna, 2014).

[2] M. Sin, R. Capote, M. W. Herman, and A. Trkov, Modelling neutron-induced reactions on $^{232-237}$U from 10 keV up to 30 MeV, Nucl. Data Sheets **139**, 138 (2017).

[3] A. D. Carlson, V. G. Pronyaev, D. L. Smith *et al.*, International evaluation of neutron cross section standards, Nucl. Data Sheets **110**, 3215 (2009).

[4] A. D. Carlson, V. G. Pronyaev, R. Capote *et al.*, Evaluation of neutron data standards, Nucl. Data Sheets **148**, 143 (2018).

[5] R. Capote, A. Trkov, M. Sin, M. Herman, A. Daskalakis, and Y. Danon, Physics of neutron interactions with ^{238}U: New developments and challenges, Nucl. Data Sheets **115**, 1 (2014).

[6] R. Capote, A. Trkov, M. Sin, M. W. Herman, and E. Sh. Soukhovitskii, Elastic and inelastic scattering of neutrons on ^{238}U nucleus, EPJ Web Conf. **69**, 00008 (2014).

[7] R. Capote, M. Sin, A. Trkov, M. W. Herman, D. Bernard, G. Noguere, A. Daskalakis, and Y. Danon, Evaluation of neutron induced reactions on U-238 nucleus, *Proc. NEMEA-7 Workshop* NEA/NSC/DOC (2014)13, NEA (OECD, 2014).

[8] R. Capote, A. Trkov, M. Sin *et al.*, IAEA CIELO evaluation of neutron-induced reactions on ^{235}U and ^{238}U targets, Nucl. Data Sheets **148**, 254 (2018).

[9] M. B. Chadwick, R. Capote, A. Trkov *et al.*, CIELO collaboration summary results: International evaluations of neutron reactions on uranium, plutonium, iron, oxygen and hydrogen, Nucl. Data Sheets **148**, 189 (2018).

[10] D. A. Brown, M. B. Chadwick, R. Capote *et al.*, ENDF/B-VIII.0: The 8th Major Release of the Nuclear Reaction Data Library with CIELO-project Cross Sections, New standards and thermal scattering data, Nucl. Data Sheets **148**, 1 (2018).

[11] P. G. Young, M. B. Chadwick, R. E. MacFarlane, P. Talou, T. Kawano, D. G. Madland, W. B. Wilson, and C. W. Wilkerson, Evaluation of neutron reactions for ENDF/B-VII: $^{232-241}$U and ^{239}Pu, Nucl. Data Sheets **108**, 2589 (2007).

[12] O. Iwamoto, Development of a comprehensive code for nuclear data evaluation, CCONE, and validation using neutron-induced cross sections for uranium isotopes, J. Nucl. Sci. Technol. (Abingdon, UK) **44**, 687 (2007).

[13] S. Goriely, S. Hilaire, A. J. Koning, M. Sin, and R. Capote, Towards a prediction of fission cross sections on the basis of microscopic nuclear inputs, Phys. Rev. C **79**, 024612 (2009).

[14] S. Goriely, S. Hilaire, A. J. Koning, and R. Capote, Towards an improved evaluation of neutron-induced fission cross sections on actinides, Phys. Rev. C **83**, 034601 (2011).

[15] E. Bauge *et al.*, Coherent investigation of nuclear data at CEA DAM: Theoretical models, experiments and evaluated data, Eur. Phys. J. A **48**, 113 (2012).

[16] P. Romain, B. Morillon, and H. Duarte, Bruyères-le-Châtel neutron evaluations of actinides with the TALYS code: The fission channel, Nucl. Data Sheets **131**, 222 (2016).

[17] M. W. Herman, R. Capote, B. V. Carlson, P. Oblozinský, M. Sin, A. Trkov, H. Wienke, and V. Zerkin, EMPIRE: Nuclear reaction model code system for data evaluation, Nucl. Data Sheets **108**, 2655 (2007).

[18] M. Herman *et al.*, *EMPIRE-3.2 Malta User's Manual, Report INDC(NDS)-0603* (IAEA, Vienna, 2013); available online at www-nds.iaea.org/publications/indc/indc-nds-0603.pdf

[19] D. Filipescu, A. Anzalone, D. L. Balabanski, S. S. Belyshev, F. Camera, M. La Cognata, P. Constantin, L. Csige, P. V. Cuong, M. Cwiok *et al.*, Perspectives for photonuclear research at the extreme light infrastructure - nuclear physics (ELI-NP) facility, Eur. Phys. J. A **51**, 185 (2015).

[20] T. Kawano, Y. S. Cho, P. Dimitriou *et al.*, Iaea photonuclear data library 2019, Nucl. Data Sheets **163**, 109 (2020).

[21] S. Goriely, P. Dimitriou, M. Wiedeking *et al.*, Reference database for photon strength functions, Eur. Phys. J. A **55**, 172 (2019).

[22] R. Capote *et al.*, RIPL–reference input parameter library for calculation of nuclear reactions and nuclear data evaluations, Nucl. Data Sheets **110**, 3107 (2009); Data available at http://www-nds.iaea.org/RIPL-3/.

[23] V. Plujko, I. Kadenko, S. Goriely, E. Kulich, O. Davidovskaya, and O. Gorbachenko, Models for photoabsorption cross section estimates, in *Proceedings of the International Conference on Nuclear Data for Science and Technology NDST2007, Nice, France* (EDP Sciences, France, 2008), https://nd2007.edpsciences.org/.

[24] V. A. Plujko, R. Capote, and O. M. Gorbachenko, Giant dipole resonance parameters with uncertainties from photonuclear cross sections, At. Data Nucl. Data Tables **97**, 567 (2011).

[25] V. A. Plujko, O. M. Gorbachenko, R. Capote, and P. Dimitriou, Giant dipole resonance parameters of ground-state photoabsorption: Experimental values with uncertainties, At. Data Nucl. Data Tables **123-124**, 1 (2018).

[26] N. Bohr, Neutron capture and nuclear constitution, Nature (London) **137**, 344 (1936).

[27] R. Capote, V. Osorio, R. López, E. Herrera, and M. Piris, *Analysis of experimental data on neutron-induced reactions and development of code PCROSS for the calculation of differential pre-equilibrium emission spectra with modelling of the level density function, Final report on research contract 5472/RB, report IAEA(CUB)-004* (International Atomic Energy Agency, Vienna, 1991).

[28] W. Hauser and H. Feshbach, The inelastic scattering of neutrons, Phys. Rev. **87**, 366 (1952).

[29] H. M. Hoffmann, J. Richert, J. W. Tepel, and H. A. Weidenmüller, Direct reactions and Hauser-Feshbach theory, Ann. Phys. (NY) **90**, 403 (1975).

[30] T. Kawano, R. Capote, S. Hilaire, and P. Chau Huu-Tai, Statistical Hauser-Feshbach theory with width-fluctuation correction including direct reaction channels for neutron-induced reactions at low energies, Phys. Rev. C **94**, 014612 (2016).

[31] M. Sin, R. Capote, M. Herman, and A. Trkov, Extended optical model for fission, Phys. Rev. C **93**, 034605 (2016).

[32] M. Sin and R. Capote, Transmission through multi-humped fission barriers with absorption: A recursive approach, Phys. Rev. C **77**, 054601 (2008).

[33] M. Sin, R. Capote, A. Ventura, M. Herman, and P. Oblozinský, Fission of light actinides: ^{232}Th(n, f) and ^{231}Pa(n, f) reactions, Phys. Rev. C **74**, 014608 (2006).

[34] B. S. Bhandari, Three-hump fission barrier in Th-232, Phys. Rev. C **19**, 1820 (1979).

[35] N. Fröman and P. O. Fröman, *JWKB Approximation, Contributions to the Theory* (North-Holland, Amsterdam, 1965).

[36] N. Fröman and Ö. Dammert, Nucl. Phys. A **147**, 627 (1970).

[37] M. Sin, R. Capote, S. Goriely, S. Hilaire, and A. J. Koning, Neutron-induced fission cross section on actinides using microscopic fission energy surfaces, in *Proceedings of the International Conference on Nuclear Data for Science and Technology NDST2007, Nice, France* (EDP Sciences, France, 2008), https://nd2007.edpsciences.org/.

[38] N. Otuka, E. Dupont, V. Semkova, B. Pritychenko *et al.*, Towards a more complete and accurate experimental nuclear reaction data library (EXFOR): International collaboration between nuclear reaction data centres (NRDC), Nucl. Data Sheets **120**, 272 (2014); data available online (e.g., at http://www-nds.iaea.org/exfor/.

[39] N. Iwamoto, K. Kosako, and T. Murata, JENDL Photonuclear Data File 2016 (JENDL/PD-2016), report **JAEA-Conf 2016-004**, 53 (2016).

[40] *Handbook of Photonuclear Data for Applications: Cross Sections and Spectra*, IAEA-TECDOC-1178 (IAEA, Vienna, 2000).

[41] R. Capote, S. Hilaire, O. Iwamoto, T. Kawano, and M. Sin, Inter-comparison of Hauser-Feshbach model codes toward better actinide evaluations, EPJ Web Conf. **146**, 12034 (2017).

[42] M. A. P. V. de Moraes and M. F. Cesar, Photonuclear cross-sections of ^{233}U using neutron capture gamma-rays, near threshold, Nuovo Cimento A **106**, 1165 (1993).

[43] G. M. Gurevich, L. E. Lazareva, V. M. Mazur, G. V. Solodukhov, and B. A. Tulupov, Giant resonance in the total photoabsorption cross section near of $Z = 90$ nuclei, Nucl. Phys. A **273**, 326 (1976).

[44] M. Herman and A. Trkov, ENDF-6 Formats Manual. Data Formats and Procedures for the Evaluated Nuclear Data File ENDF/B-VI and ENDF/B-VII, CSEWG Document ENDF-102, Report BNL-90365-2009, Rev.2, SVN Commit 85 (2012).

[45] S. Goriely, E. Khan, and M. Samyn, Microscopic HFB + QRPA predictions of dipole strength for astrophysics applications, Nucl. Phys. A **739**, 331 (2004).

[46] B. L. Berman, J. T. Caldwell, E. J. Dowdy, S. S. Dietrich, P. Meyer, and R. A. Alvarez, Photofission and photoneutron cross sections and photofission neutron multiplicities for ^{233}U, ^{234}U, ^{237}Np, and ^{239}Pu, Phys. Rev. C **34**, 2201 (1986).

[47] J. T. Caldwell, E. J. Dowdy, B. L. Berman, R. A. Alvarez, and P. Meyer, Giant resonance for the actinide nuclei: Photoneutron and photofission cross sections for ^{235}U, ^{236}U, ^{238}U, and ^{232}Th, Phys. Rev. C **21**, 1215 (1980).

[48] A. Veyssiere, H. Beil, R. Bergere, P. Carlos, and A. Lepretre, A study of the photofission and photoneutron processes in the giant dipole resonance of ^{232}Th, ^{238}U, and ^{237}Np, Nucl. Phys. A **199**, 45 (1973).

[49] R. Bergere, H. Beil, B. Carlos, A. Veyssiere, and A. Lepretre, Study of the giant resonance of fissile nuclei, *Conf. Nucl. Structure Studies, Sendai, Japan*, 273 (1972).

[50] O. L. Goncalez, L. P. Geraldo, and R. Semmler, Measurement of neutron photoproduction cross sections for ^{232}Th and ^{238}U using capture gamma rays, Nucl. Sci. Eng. **132**, 135 (1999).

[51] P. A. Dickey and P. Axel, ^{238}U and ^{232}Th Photofission and Photoneutron Emission near Threshold, Phys. Rev. Lett. **35**, 501 (1975).

[52] O. Y. Mafra, S. Kuniyoshi, and J. Goldemberg, Intermediate structure in the photoneutron and photofission cross sections in u-238 and th-232, Nucl. Phys. A **186**, 110 (1972).

[53] M. A. P. V. de Moraes and M. F. Cesar, Photofission cross sections of ^{233}U and ^{239}Pu near threshold induced by gamma rays from thermal neutron capture, Nucl. Instr. & Methods A **277**, 467 (1989).

[54] A. S. Soldatov and G. N. Smirenkin, Yield and cross section for fission of odd nuclei by gamma-rays with energy up to 11 MeV. Results of relative measuring of photofission yields and cross sections for nuclei ^{233,235}U, ^{237}Np, ^{239,241}Pu, and ^{241}Am in the energy region 5–11 MeV, Yad. Fiz. **55**, 3153 (1992) (in Russian).

[55] V. E. Zhuchko, Ya. B. Ostapenko, G. N. Smirenkin, A. S. Soldatov, and Ya. M. Tsipenyuk, Investigation of probability of the near-threshold fission of Th, U, Np, Pu, Am isotopes by

bremsstrahlung gamma-quanta, Yad. Fiz. **28**, 1170 (1978) (in Russian).

[56] J. R. Huizenga, K. M. Clarke, J. E. Gindler, and R. Vandenbosch, Photofission cross sections of several nuclei with mono-energetic gamma rays, Nucl. Phys. **34**, 439 (1962).

[57] A. S. Soldatov, Photofission cross section of uranium-234 in the energy region from 5 to 9 MeV and its comparison with the data for thorium-232 and neptunium-237 in subbarrier region, Yad. Fiz. **56**, 16 (1993) (in Russian).

[58] L. J. Lindgren, A. S. Soldatov, and Yu. M. Tsipenyuk, Under-barrier photofission of U-234, Yad. Fiz. **32**, 335 (1980) (in Russian).

[59] C. D. Bowman, I. G. Schroder, K. C. Duvall, and C. E. Dick Subthreshold photofission of U-235 and Th-232, Phys. Rev. C **17**, 1086 (1978).

[60] H. Ries, U. Kneissl, G. Mank, H. Stroher, W. Wilke, R. Bergere, P. Bourgeois, P. Carlos, J. L. Fallou, P. Garganne, A. Veyssiere, and L. S. Cardman, Absolute photofission cross sections of U-235, 238 measured with tagged photons between 40 and 105 MeV, Phys. Lett. B **139**, 254 (1984).

[61] R. A. Anderl, M. V. Yester, and R. C. Morrison, Photofission cross sections of U-238 and U-235 from 5.0 to 8.0 MeV, Nucl. Phys. A **212**, 221 (1973).

[62] A. M. Khan and J. W. Knowles, Photofission of Th-232, U-238, and U-235 near threshold using a variable energy beam of gamma-rays, Nucl. Phys. A **179**, 333 (1972).

[63] C. D. Bowman, C. F. Auchampaugh, and S. C. Fultz, Photodis-integration of ^{235}U, Phys. Rev. **133**, B676 (1964).

[64] Yu. B. Ostapenko, G. N. Smirenkin, A. S. Soldatov, V. E. Zhuchko, and Yu. M. Tsipenyuk, Yields and cross sections of photofission for isotopes Th, U, Np, and Am in energy range from 4.5 MeV to 7.0 MeV, Vop. At. Nauki i Tekhn., Ser. Yadernye Konstanty **30**, 3 (1978) (in Russian).

[65] V. E. Zhuchko, Yu. B. Ostapenko, A. S. Soldatov, and Yu. M. Tsipenyuk, Restoration of photofission cross-sections from bremsstrahlung experiments, Nucl. Instr. Meth. Phys. Res. **136**, 373 (1976).

[66] M. V. Yester, R. A. Anderl, and R. C. Morrison, Photofission cross sections of Th-232 and U-236 from threshold to 8 MeV, Nucl. Phys. A **206**, 593 (1973).

[67] A. S. Soldatov and G. N. Smirenkin, Yield and cross section of ^{232}Th and ^{236}U fission induced by gamma-quanta with energy below 11 MeV, Yad. Fiz. **58**, 224 (1995) (in Russian).

[68] V. E. Zhuchko, Yu. B. Ostapenko, G. N. Smirenkin, A. S. Soldatov, and Yu. M. Tsipenyuk, Experimental investigations of the effect of the 'isomer shelf' in photofission cross sections of heavy nuclei, Yad. Fiz. **28**, 1185 (1978) (in Russian).

[69] L. Csige, D. M. Filipescu, T. Glodariu, J. Gulyas, M. M. Gunther, D. Habs, H. J. Karwowski, A. Krasznahorkay, G. C. Rich, M. Sin, L. Stroe, O. Tesileanu, and P. G. Thirolf, Exploring the multihumped fission barrier of ^{238}U via sub-barrier photofission, Phys. Rev. C **87**, 044321 (2013).

[70] A. Lepretre, R. Bergere, P. Bourgeois, P. Carlos, J. Fagot, J. L. Fallou, P. Garganne, A. Veyssiere, H. Ries, R. Gobel, U. Kneissl, G. Mank, H. Stroher, W. Wilke, D. Ryckbosch, and J. Jury, Absolute photofission cross sections for ^{232}Th and ^{235,238}U measured with monochromatic tagged photons (20 MeV $< E_\gamma <$ 110 MeV), Nucl. Phys. A **472**, 533 (1987).

[71] A. Manfredini, M. Muchnik, L. Fiore, C. Ramorino, H. G. De Carvalho, R. Bosch, and W. Wolfli, Results on the cross section of ^{238}U fission induced by low energy monoenergetic gamma rays, Nuovo Cimento B **44**, 218 (1966).

[72] Yu. B. Ostapenko, G. N. Smirenkin, A. S. Soldatov, and Yu. M. Tsipenyuk, Isomer shelf in the photofission of Th-232 and U-238, Phys. Rev. C **24**, 529 (1981).

[73] I. S. Koretskaya, V. L. Kuznetsov, L. E. Lazareva, V. G. Nedoresov, and N. V. Nikitina, Photofission cross sections for the nuclei Am-241 and Am-243 in the region of the $E1$ giant resonance, Yad. Fiz. **30**, 910 (1979) (in Russian).

[74] J. D. T. Arruda Neto, S. B. Herdade, B. S. Bhandari, and I. C. Nascimento, Electrofission and photofission of U-238 in the energy range 6–60 MeV, Phys. Rev. C **14**, 1499 (1976).

[75] N. S. Rabotnov, G. N. Smirenkin, A. S. Soldatov, L. N. Usachev, S. P. Kapitza, and Yu. M. Tsipenyuk, Photofission of Th-232, U-238, Pu-238, Pu-240, and Pu-242 nuclei and structure of fission barrier, Yad. Fiz. **11**, 508 (1970) (in Russian).

[76] L. Katz, A. P. Baerg, and F. Brown, Photofission in heavy elements, Second Internat. At. En. Conf., Geneva, **15**, 188 (1958).